Interaction of Methanol with Well-Defined Ceria Surfaces: Reflection/Absorption Infrared Spectroscopy, X-ray Photoelectron Spectroscopy, and Temperature-Programmed Desorption Study

A. Siokou and R. M. Nix*

Department of Chemistry, Queen Mary and Westfield College, University of London, London E1 4NS, U.K.

Received: April 2, 1999; In Final Form: June 21, 1999

The adsorption of methanol on ordered epitaxial layers of cerium oxides grown on a Cu(111) substrate has been studied using X-ray photoelectron spectroscopy (XPS), low-energy electron diffraction (LEED), temperature-programmed desorption (TPD), and Fourier transform reflection/absorption infrared spectroscopy (FT-RAIRS) measurements. The oxide films exhibit a LEED pattern characteristic of a CeO_2(111)-like structure, but the Ce/O stoichiometry achieved is strongly dependent on the exact pretreatment and film history. Grazing emission XPS also indicates that some Ce^{3+} ions are still present in the surface layers at 300 K after oxidation treatments. Methanol adsorbs dissociatively at 300 K, with a relatively high sticking probability, to yield surface methoxy species. The IR spectra of the methoxy species, in particular the C—O stretch frequency, provide information about their coordination to the oxide surface, the presence of surface oxygen vacancies, and the general level of oxidation of the film. The methoxy species are stable on the (111)-type terraces of thicker (>5 ML) oxide films to temperatures in excess of 550 K but then decompose at about 585 K to yield predominantly H_2 and CO with some simultaneous evolution of formaldehyde and water. A substantial number of more coordinatively unsaturated cerium ions exist at and near the periphery of oxide islands on films of a submonolayer oxide coverage and on aggregated films of higher oxide coverage (between 1 and 5 ML). When the substrate is well-oxidized, then some of the methoxy species adsorbed at such sites are readily oxidized to the formate species while the decomposition temperature of the remaining methoxy groups in this peripheral region is lowered to about 560 K and their decomposition yields a higher proportion of formaldehyde than is seen for the (111) terrace sites.

Introduction

Oxides of the lanthanide metals have featured prominently in the search for new and improved catalysts for a range of chemical and environmental processes. Ceria, in particular, is now a major component of three-way auto exhaust catalysts, in which context it has been attributed roles which are related to its oxygen storage capacity,[1] its contribution to the stabilization of the surface area of the alumina washcoat,[2] the stabilization of the precious metal dispersion,[3] and the promotion of the water gas shift reaction.[4] Another active area of research into catalysis by oxides is the production of functionalized hydrocarbons from common feedstocks; this research extends to processes such as the direct conversion of methane and synthesis gas ($CO-CO_2-H_2$) chemistry[5,6] in which many of the reactions involve the production and interconversion of simple C_1 molecules such as methane, methanol, formaldehyde, and formic acid. Cerium-containing catalysts have once again attracted attention in this area; examples of reactions for which they have been the subject of study range from methanol synthesis (over catalysts derived from Cu−Ce intermetallic compounds[7]) to the oxidation of methane to CO (over Ce−Cu−O composite catalysts[8]).

For these and other reasons, there is much current interest in the fundamental surface properties of the lanthanide oxides and in particular in the surface chemistry of ceria. An increasingly common approach to the study of these oxides, which cannot readily be produced in a single crystal form, is through the growth of the oxide as thin films on metallic substrates. In such systems, submonolayer coverages and thin films of the oxide on the metal may act as models for the highly dispersed oxide in mixed metal/oxide catalyst formulations, while thicker films are used as model substrates for fundamental studies of the surface chemistry of the bulk oxide.

In this work, well-defined ceria overlayers were prepared on a Cu(111) substrate by the low-pressure oxidation of cerium predeposited by vacuum evaporation. The growth and characteristics of the ceria films, as well as their behavior during thermal treatment, have been investigated using surface-sensitive techniques such as low-energy electron diffraction (LEED) and X-ray photoelectron spectroscopy (XPS). The adsorption of methanol has been further studied using a combination of temperature-programmed desorption (TPD) and reflection/absorption infrared spectroscopy (RAIRS) measurements; as we will demonstrate, the study of methanol serves two purposes in that (i) it enables the surface chemistry of methanol itself to be elucidated (particularly with respect to its dissociation and oxidation pathways) and (ii) the methanol may be used as a probe molecule to study the reactivity and surface structure of the ceria surfaces.

Experimental Section

The experiments were carried out in an ultrahigh vacuum (UHV) system that has been described in detail elsewhere.[9] The main analytical chamber is equipped with a 100 mm hemi-

* To whom correspondence should be addressed. Phone: +44 171 775 3273. Fax: +44 181 981 8745. E-mail: r.m.nix@qmw.ac.uk.

10.1021/jp991127h CCC: $18.00
Published on Web 07/30/1999

spherical analyzer, electron gun, and Mg Kα X-ray source for Auger electron spectroscopy (AES) and XPS studies; a quadrupole mass spectrometer for residual gas analysis and TPD studies; and rear-view LEED optics. A second vessel forms a small cell for RAIRS studies and dosing gases at pressures up to 0.1 Torr. The two interconnected vacuum vessels are independently pumped by a combination of ion, diffusion, and titanium sublimation pumps, and both have a base pressure of ca. 1×10^{-10} Torr.

The Cu(111) crystal was initially cleaned using extensive Ar^+ bombardment (700 eV, 12−14 μA), at both room temperature and 773 K, followed by annealing at 973 K for about 5 min to restore the surface order. This latter requirement was confirmed by LEED, with a sharp Cu(111)-(1×1) pattern evident after the cleaning procedure. The only impurity detected by XPS after cleaning was trace amounts of surface carbon.

The cerium dosing source was purpose-built for this work and consisted of 99.9% Ce held in a resistively heated tungsten wire basket. The source was enclosed in a molybdenum cage that could be separately outgassed. The cerium atom flux was monitored using a mass spectrometer with direct line-of-sight to the evaporator and controlled by regulating the heating current. The amount of evaporated cerium was also quantitatively estimated using XPS, from an analysis of the attenuation of the Cu $2p_{3/2}$ signal, and assuming uniform oxide layer growth.

The interpretation of Ce 3d XPS data has been a long-running controversy and only relatively recently has a general consensus emerged about the peak assignments. The data of this work are in very good agreement with the data of these more recent studies.[10−12] Briefly, each spin−orbit component of the Ce 3d XP spectrum is dominated by three features in the case of CeO_2 but contains only two main peaks for Ce_2O_3; the interpretation of the complete Ce 3d spectrum of a partially reduced ceria sample will therefore imply the complete analysis of 10 peaks in total when all spin−orbit components are taken into account. The value of the stoichiometric coefficient (x of CeO_x) can be estimated quantitatively either from an analysis of the relative intensities of the Ce 3d and O 1s spectra or from a detailed deconvolution of the Ce 3d emission profile, although it needs to be recognized that both methods yield an *average* stoichiometry (albeit a surface-weighted average) for the XPS-sampled region. Both approaches were used in this work and reasonable agreement (better than ±0.05) obtained for the majority of samples. The deconvolution method involved the initial optimization of fits for samples in which cerium was present almost exclusively in one or another of the two oxidation states in order to generate photoemission profiles characteristic of the individual oxidation states. Other spectra were then analyzed by fitting the experimental data using linear combinations of the two profiles, with only fractional changes to the relative positions and variation of the complete profile intensities being permitted. Only the values of oxide stoichiometry obtained using this latter deconvolution method are quoted in subsequent sections.

Methanol was purified by drying over a molecular sieve and dissolved permanent gases removed by freeze/pump/thaw cycles. Unless specifically mentioned, all methanol exposures were carried out using background pressures in the range 5×10^{-8} to 5×10^{-7} Torr and with the substrate at a temperature of 300−340 K.

Results

Deposition and Oxidation of Ce on Cu(111) at Ambient Temperatures. The main purpose of this study was to characterize the structure and reactivity of the cerium oxide overlayers after the oxidation of the deposited cerium, and little attention was given to the interface properties of the bimetallic Ce/Cu system. Previous reports[13] indicate that extensive alloying can occur during the deposition of Ce onto polycrystalline Cu substrates, and while this was not immediately evident in this work on Cu(111), the copper substrate was always maintained at ambient temperatures during the initial deposition of Ce, and this deposition was immediately followed by a rapid oxidation of the deposited layers to minimize any possible effects arising from intermixing of the two metals.

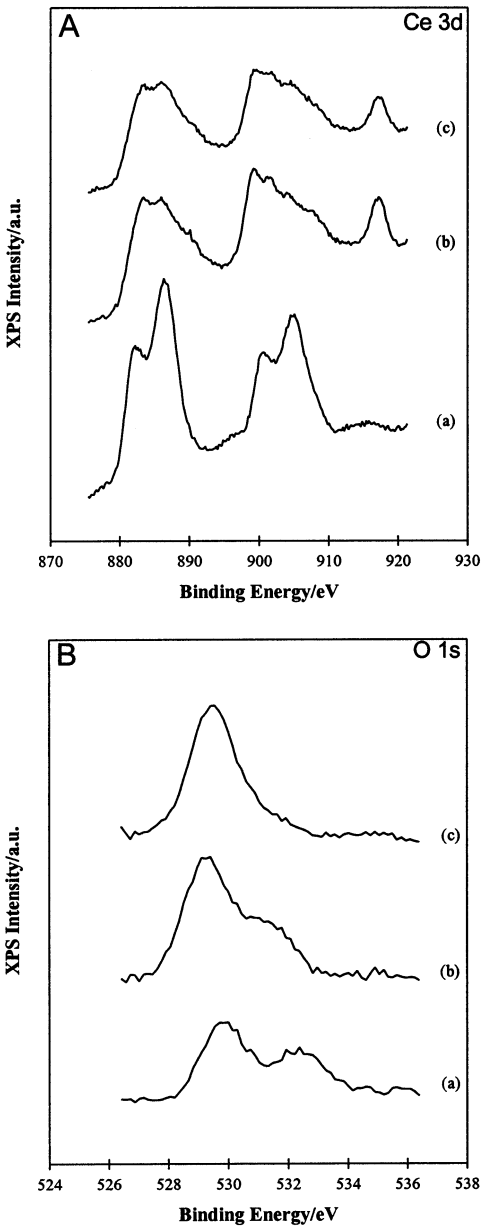

Figure 1. (A) Ce 3d and (B) O 1s XP spectra recorded during the initial oxidation of freshly deposited cerium at 300 K and after annealing of the 10 ML of ceria film: (a) 2 L of O_2; (b) 170 L of O_2; (c) annealed at 820 K for 3 min.

All the deposited Ce films exhibited a fast uptake of oxygen from molecular O_2 at ambient temperatures, leading to a rapid transformation of Ce from the zerovalent metallic state to Ce^{3+} (Ce_2O_3) throughout the XPS sampling depth, even for relatively low oxygen exposures (spectrum a of Figure 1A). At this stage of oxidation, the O 1s peak is usually composed of two peaks, one at ca. 529.8 eV and another smaller peak at ca. 532 eV (spectrum a of Figure 1B). The latter peak is believed to

correspond to hydroxide or carbonate species formed by adventitious adsorption; the evidence that this peak is in part due to carbonate comes from the observed concurrent reduction in intensity of this O 1s shoulder and a weak C 1s peak (286 eV) following heating to 473 K and above and from the observation in control TPD experiments of some CO_2 desorption giving rise to a 44 amu desorption peak with a maximum above 500 K. The surface localization of the species responsible for the higher binding energy O 1s peak has been confirmed by comparison of spectra acquired at near-normal and grazing emission angles that show this peak to be much more prominent at grazing emission angles.

Further oxidation of freshly evaporated Ce films at 300 K does not readily lead to complete conversion to Ce^{4+}; instead the Ce 3d spectrum apparently contains a combination of Ce^{3+} and Ce^{4+} characteristics even after high oxygen doses (see, for example, spectrum b of Figure 1A). This coexistence of cerium in both Ce^{3+} and Ce^{4+} oxidation states indicates that the overall stoichiometry of the limiting oxide (CeO_x) achieved at ambient temperatures must have an x value in the range 1.50−2.00. In the specific case of the film from which spectrum b in Figure 1A was obtained, the final stoichiometry is $CeO_{1.84}$. In respect of the mixed valence exhibited by films obtained at ambient temperatures, these data are consistent with those obtained in previous studies of the low-pressure oxidation of Ce films evaporated on Pd(111),[10] Rh(111),[11] and Pt(111)[14] and the oxidation of polycrystalline Ce foil.[15] In agreement with our previous work, we propose that the film is rapidly oxidized to Ce_2O_3 and with further oxidation at ambient temperatures a thin capping surface layer that is rather closer in stoichiometry to CeO_2 is formed.[10]

During extended dosing of a freshly evaporated film with oxygen, the main O 1s peak shifts continuously to lower binding energy; this behavior is illustrated in Figure 1B for a 10 ML Ce film, for which the O 1s binding energy attains a value of ca. 529.8 eV for a Ce_2O_3 stoichiometry (as noted above) and then continues to shift and ultimately attains a value of ca. 529.4 eV for exposures over 100 L of O_2. The higher binding energy O 1s feature "tracks" the main peak and, in this particular case, contributes about 30% of the total O 1s integrated intensity for the highest exposures.

The oxidized Ce layers formed at ambient temperatures, in the manner described above, showed no long-range order with only a faint Cu(111) substrate LEED pattern visible at low Ce coverages and a diffuse background evident at higher Ce coverages.

Stepwise Annealing of the Oxidized Films and Reoxidation Characteristics. Annealing of films prepared by oxidation of the freshly deposited Ce at ambient temperatures has several consequences; this is again illustrated for a 10 ML film in spectrum c of Figure 1A and spectrum c of Figure 1B. First, the higher binding energy O 1s feature begins to lose intensity after annealing to 473 K and is completely removed by heating to 673 K. Above 473 K the main O 1s peak maximum shifts back to 529.6 eV. Heating above 673 K also causes changes in the Ce 3d spectrum; there is an increase in the relative intensity of the features characteristic of Ce^{3+}, indicating that the cerium in the surface layers is being reduced (in this particular case the average stoichiometry falls from $CeO_{1.84}$ to $CeO_{1.80}$). These latter changes are attributed mainly to the diffusion of oxygen into subsurface regions of the film, as previously reported for cerium oxide films grown on Pd(111).[10] In the case of films subjected to milder oxygen exposures than the film of Figure 1, the initial heating can apparently result in a complete reversion of the cerium oxidation state to Ce^{3+}, as evidenced from XPS. TPD experiments confirm that there is no desorption of cerium or molecular oxygen over the temperature range studied, although, as noted earlier, control experiments on freshly oxidized films did reveal some CO_2 desorption in a peak above 500 K and a very small amount of H_2O desorption at ca. 450 K (by contrast, virtually no CO_2 desorption was seen from preannealed oxide films, although some H_2O desorption was still evident at ca. 450 K).

Reoxidation of annealed films, by reexposure to O_2 at ambient temperatures, reverses the effects seen during the initial annealing with an increase in oxygen concentration and a concomitant conversion of Ce^{3+} to Ce^{4+}; furthermore, the final oxidation level attained by reoxidation generally exceeded that obtained during the very initial oxidation procedure. For thicker oxide films (>5 ML), it was found that repeating this annealing/reoxidation treatment several times proved to be an effective method for preparing films with a stoichiometry very close to that of CeO_2. Figure 2 illustrates the reoxidation process for a thick oxide film that has been built up using a number of cycles of Ce deposition and oxidation. The Ce 3d spectrum recorded after the initial oxidation of the Ce deposited in the final cycle (trace a) clearly shows features due to Ce^{3+} in addition to those attributable to Ce^{4+} (and the overall stoichiometry is estimated as $CeO_{1.88}$). Reoxidation by exposure to 30 L of O_2 at 300 K transforms the Ce 3d profile to one that is much more consistent with the presence only of Ce^{4+} (spectrum b of Figure 2A), and there is a significant increase in the O 1s peak intensity(spectrum b of Figure 2B), the overall stoichiometry of the resultant oxide being $CeO_{1.98}$. Such reoxidized films also exhibit greater stability with respect to any tendency to reduce during temperature treatments; spectra c and d of Figure 2A indicate an oxide stoichiometry of $CeO_{1.92}$ and $CeO_{1.83}$ after annealing at 690 and 930 K, respectively. By contrast, for thinner films we did not manage to attain a stoichiometry close to the dioxide even after repeating the same reoxidation procedure. Once again, this behavior is very similar to that observed for cerium oxides on palladium where the anomalous behavior of the thinner films was attributed to the immediate influence of the metal/oxide interface.[10]

Even with the thicker oxide films, however, we would note that there is invariably some Ce^{3+} closely localized to the vacuum interface (i.e., the surface is partially reduced, a condition that is also apparent from the RAIRS data presented below). In XPS this is demonstrated by a direct comparison of Ce 3d spectra recorded at near-normal and grazing emission angles (Figure 3).

In addition to the effects mentioned above, annealing the oxide films to high temperatures can result in other more substantial changes. The onset of these changes is marked by the intensity of the Cu 2p signal starting to increase, while that of the Ce 3d and O 1s peaks begins to decrease. These changes suggest that the oxide film begins to aggregate on the Cu(111) surface. This phenomenon is shown clearly in Figure 4 where the variation of the Cu 2p and the Ce 3d signal intensities have been plotted as a function of annealing temperature for 4 and 15 ML of oxide films. From these data it is clear that the thicker 15 ML oxide film is stable to temperatures in excess of 773 K, whereas annealing the thinner (4 ML) oxide layer results in a decrease in Ce 3d intensity starting at about 650 K, indicating that this film is less stable to the heating treatment compared to the thicker oxide film.

After annealing multilayer oxide films at 700 K (for ca. 5 min), we were able to detect a new LEED pattern. The pattern

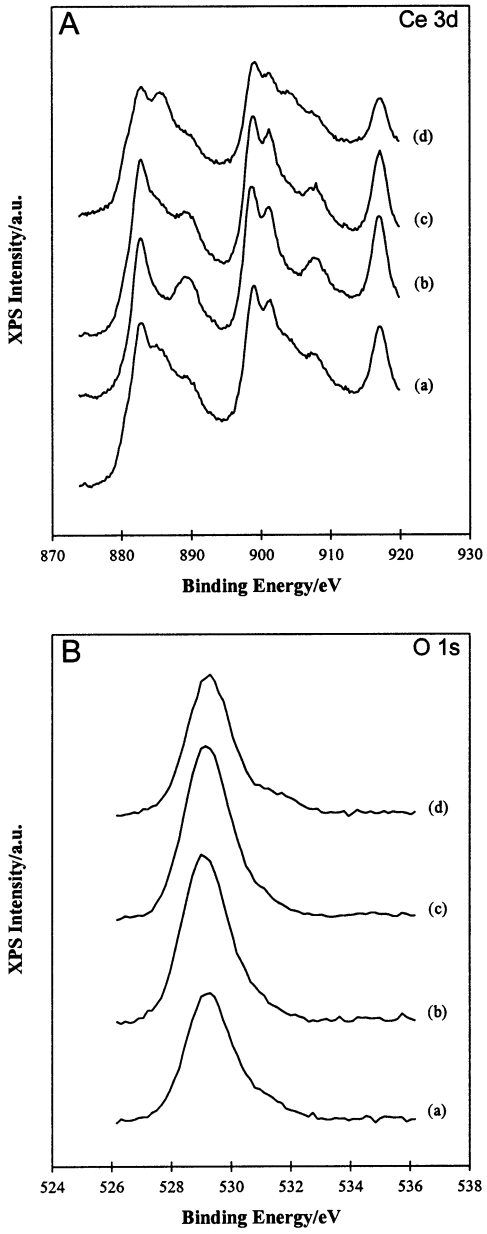

Figure 2. (A) Ce 3d and (B) O 1s XP spectra of a 9 ML thick oxide film prepared in steps: (a) after the last cycle of Ce evaporation and oxidation (30 L of O_2) at 300 K; (b) annealed at 670 K and then reoxidized at 300 K (30 L of O_2); (c) annealed at 690 K; (d) annealed at 930 K.

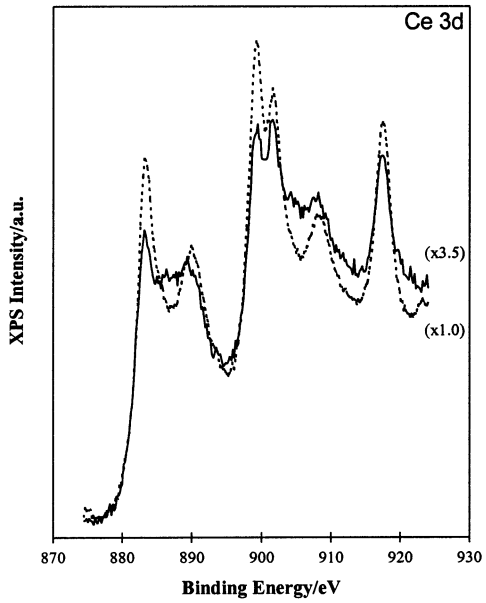

Figure 3. Ce 3d XP spectra for normal (dashed line) and grazing (solid line) emission for a well-oxidized (preoxidized) film.

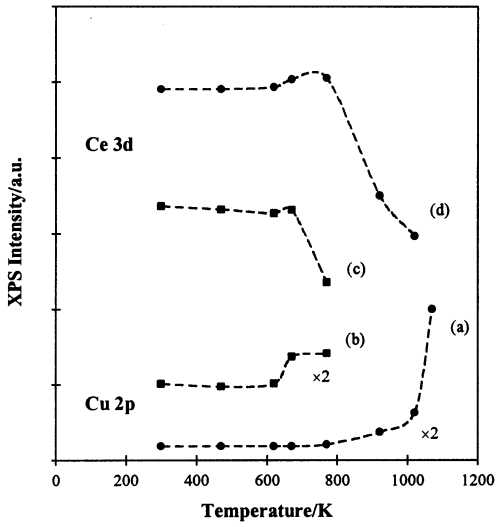

Figure 4. Variation of Cu 2p (a, b) and Ce 3d (c, d) XPS peak intensity with annealing temperature for well-oxidized (preoxidized) films of 4 ML (■) and 15 ML (●) coverage.

shown in Figure 5A was obtained by annealing a 1.3 ML of oxide film, and the diffraction spots from the Cu(111) substrate are still visible, whereas Figure 5B shows the LEED pattern from a much thicker 20 ML oxide layer. This new pattern, which is characteristic of the cerium oxide, corresponds to a $(1.5 \times 1.5) \pm 0.05$ overlayer with respect to the underlying Cu(111) surface and hence to a structure with the same hexagonal symmetry and a lattice parameter of $a = 3.84 \pm 0.11$ Å. For thick (>10 ML) oxide films this structure persists even after annealing up to 1000 K, although at higher temperatures spots attributable to the Cu(111) substrate can appear on the pattern, indicating the extended aggregation of the oxide layer. It appears therefore that even after the film has started to aggregate, the oxide still forms long-range ordered islands that retain a distinct epitaxial relationship with the substrate.

For thicker films (e.g., 10 ML and above), the quality of the LEED pattern from the ordered oxide overlayer was very much improved by preparing the oxide in steps. More specifically, well-ordered thick films could best be prepared by successive cycles in which oxide layers of ca. 2 ML thickness were deposited by Ce deposition and ambient oxidation, and these were then annealed and again reoxidized at 300 K before the next layer was deposited.

Adsorption and Surface Reactions of CH_3OH on Ceria. The adsorption of methanol has been used both as a probe of the surface structure and as a means of studying the reactivity of the ordered cerium oxide films. To permit comparison between the properties of films of various thickness, studies have been carried out on high (>10 ML of CeO_x), intermediate (~3ML of CeO_x), and submonolayer (<1ML CeO_x) coverages of the oxide. The films were prepared and characterized as described in the previous section. Unless specifically mentioned, all the oxide films in this section have been subjected to at least one reoxidation procedure to enhance their stability with respect to annealing treatments. All films gave a reasonably sharp CeO_x-(111) LEED pattern or, at the intermediate and submonolayer

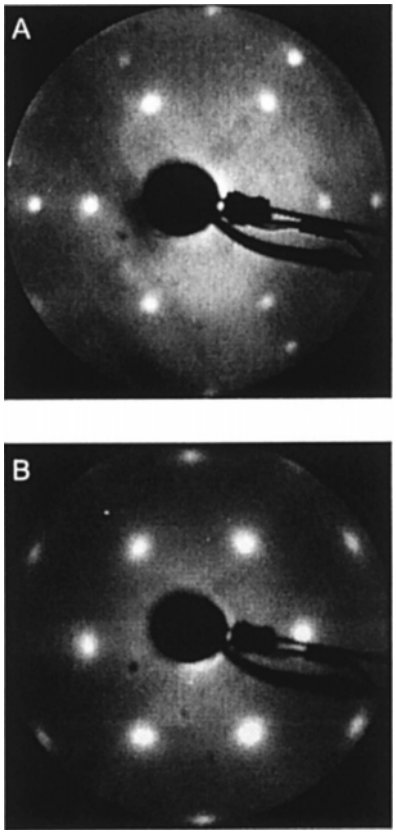

Figure 5. LEED patterns (80−85 eV) from annealed ceria films: (A) 1.3 ML of CeO_x showing an inner ring of first-order diffraction spots from the oxide surrounded by an outer ring (with intensities exhibiting 3-fold symmetry) from the Cu(111) substrate; (B) 20 ML of CeO_x showing only spots attributable to the oxide (and some spot broadening).

coverages, a superposition of the Cu(111) and CeO_x(111)-(1.5 × 1.5) patterns.

In the following sections we will use the term *annealed* for those oxide films that were heated in UHV after the last reoxidation treatment. Annealing was carried out at 800 K for the thickest films, but the annealing temperature was reduced to around 650 K for oxide films of lower coverages (up to 5 ML). The term *preoxidized* is used to describe those oxide films that were not annealed between reoxidation and exposure to methanol.

Prior to presentation of the results of this study, it is useful to note that previous work indicates that dissociative adsorption of methanol on metal oxides involves cation/anion site pairs (acid/base Lewis pairs) and that the critical requirement for dissociation to occur is the presence of a vacant coordination site on the surface cation; by comparison, the coordination environment of oxygen anions is apparently less critical.[16] Lamotte et al.[17] have also demonstrated that only $^{18}O-CH_3$ species are produced after $CH_3{}^{18}OH$ adsorption on ceria, indicating that dissociative adsorption proceeds only by OH bond cleavage on this oxide, i.e., that the adsorption process is best represented by the equation

$$CH_3O-H + O_s \rightarrow CH_3O_{(ads)} + O_sH \qquad (1)$$

where O_s is used to represent a surface oxygen ion. As will be demonstrated, our own data fully support this model for the initial interaction of methanol with ceria, and this therefore forms a useful basis for the presentation and discussion of the results that follow.

XPS Data. The adsorption of methanol was accompanied by changes in both the C 1s and O 1s spectra; these changes were most evident in the grazing emission spectra, as would be expected for a surface-adsorbed species. While the exact binding energies depended on the nature of the oxide film, the essential characteristics were similar in all cases with dosing at ambient temperatures being accompanied by the appearance of (1) a new C 1s peak at ca. 286 eV binding energy (spectrum a of Figure 6A) and (2) a new O 1s peak with a peak energy of ca. 532 eV (i.e., to higher binding of the main oxide O 1s peak). In general, these two new peaks increased in intensity with methanol exposures of up to ca. 20 L during dosing at 300 K, while all trace of the surface species was removed by subsequent heating in a vacuum to above 550 K (see, for example, spectrum c of Figure 6A). There was no evidence from the XPS data either for multiple surface species or for any temperature-induced transformations in the nature of the species responsible for the additional C 1s and O 1s peaks. A provisional assignment of these peaks may therefore be made with both the C 1s and O 1s peaks being associated with surface methoxy species generated by dissociative methanol adsorption.

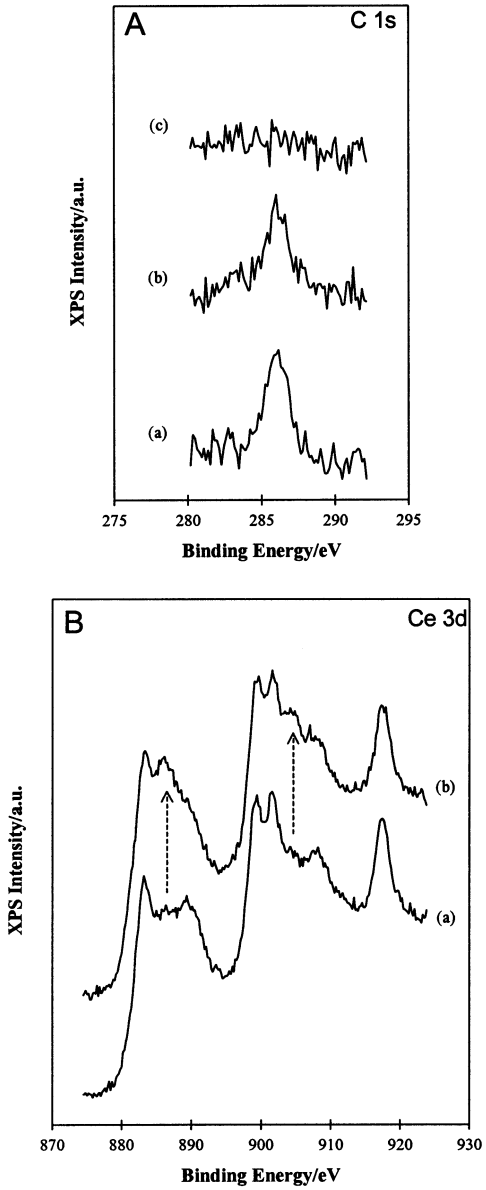

Figure 6. (A) Normal emission C 1s XP spectra for a well-oxidized 10 ML film (a) after dosing 5 L of CH_3OH at 300 K and after subsequent heating to (b) 410 K and (c) 570 K. (B) Grazing emission Ce 3d spectra from the same oxide (a) before and (b) after dosing 5 L of CH_3OH at 300 K.

In addition to the changes reported above, exposure to methanol also consistently led to some subtle changes in the Ce 3d spectra, specifically, an appearance of enhanced Ce^{3+} characteristics that are again more obvious at grazing emission angles (Figure 6B).

LEED Data. No new LEED patterns were observed when methanol was progressively adsorbed onto an ordered oxide surface at ambient temperatures, indicating that the adsorbed methoxy groups do not exhibit any long-range ordering.

RAIRS Data. In this work, the main IR absorption features initially apparent in the RAIRS spectra after methanol exposure at 300 K for all the various types of oxide film correspond to vibrational modes of methoxy species [specifically, the $\nu_a(CH_3)$, $\nu_s(CH_3)$, ν(CO) bands] and there was no evidence for any molecular methanol adsorption at ambient temperatures. The RAIRS measurements thus support the assertion that methanol dissociates completely when adsorbed at ambient temperatures on the CeO_x(111) surface and enable us to confirm the identity of the major species existing on the surface after dissociation; namely, surface methoxy (CH_3O) groups and, by implication, some form of surface "H" such as hydroxy groups. However, no vibrational modes originating from surface hydroxy groups were observed. Isolated (i.e., noninteracting) hydroxy groups, with the O—H bond oriented nearly vertical to the surface, would be expected to give rise to a sharp absorption band at about 3600 cm^{-1}, but if the O—H bonds are substantially inclined to the surface normal and the H atoms are involved in hydrogen bonding interactions with neighboring species, then the absorption band would be both weak and broadened, and it would then be very difficult to distinguish it in our IR spectra.

The detailed nature of the IR spectra observed for the Cu(111) surface covered with cerium oxide films of varying thickness will now be considered.

1. The 10−20 ML Oxide. When methanol is dosed onto thick oxide films at ambient temperatures, there are two principal sets of bands in the RAIRS spectra, those located in the range 1120−1000 cm^{-1} representing the ν(CO) vibrational mode of adsorbed methoxy species and a set of bands between 2925 and 2780 cm^{-1} representing the $\nu(CH_3)$ modes of the same species.

After dosing methanol at 320 K onto a well-oxidized *annealed* film (Figure 7a), we detect three peaks in the ν(CO) region, located at 1105, 1058, and 1027 cm^{-1}. All three bands correspond to ν(CO) vibrational modes of surface methoxy species, differing in their bonding geometries on the oxide surface. The band at 1105 cm^{-1} is attributed to on-top-bonded methoxy species (type I), while the bands at 1058 and 1028 cm^{-1} may be assigned to bridge-bonded (type II) and triply bonded (type III) methoxy species, respectively [see Discussion], where the specified geometry refers to the manner in which the oxygen atom of the methoxy group is coordinated to surface cerium cations. The absorption bands of the C—H stretch region are rather less well-defined, being both rather broad and very weak, but both symmetric methyl stretches ($\nu_s(CH_3)$, at around 2800 cm^{-1}) and asymmetric methyl stretches ($\nu_a(CH_3)$, at around 2920 cm^{-1}) are readily detectable. Close inspection of a large number of such spectra and comparison with the literature suggest that each "band" is actually composed of several overlapping contributions from the various different methoxy species. The main peak in the $\nu_s(CH_3)$ region is at 2808 cm^{-1}, but the band profile includes two small shoulders at 2798 and 2787 cm^{-1} while the main feature of the asymmetric stretch is at 2912 cm^{-1} with a small shoulder at 2925 cm^{-1}. The effects of postoxidation at 320 K in this situation are not particularly dramatic (Figure 7b); the main peak (type I methoxy species)

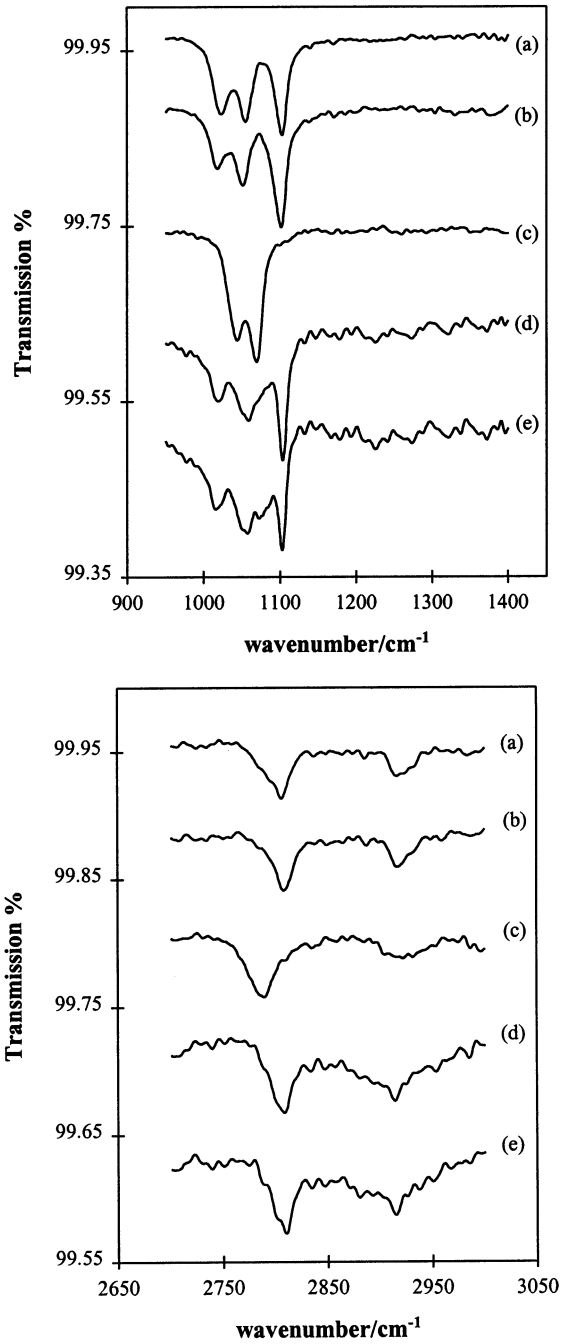

Figure 7. RAIRS spectra recorded at 300 K from a 10 ML of oxide film: (a) an annealed film dosed with CH_3OH to saturation coverage; (b) an annealed film dosed with CH_3OH to saturation coverage and subsequent oxidation; (c) an annealed heavily reduced film dosed with CH_3OH to saturation coverage at 390 K; (d) a preoxidized film dosed with CH_3OH to saturation coverage; (e) a preoxidized film dosed with CH_3OH to saturation coverage and subsequent oxidation.

in the ν(CO) region gains intensity at the expense of the two other peaks, which also shift slightly toward lower wavenumbers from 1057 to 1054 cm^{-1} and from 1027 cm^{-1} to 1021 cm^{-1}, respectively. The $\nu_s(CH_3)$ peak shifts from 2808 to 2811 cm^{-1}, while the $\nu_a(CH_3)$ peak at 2912 cm^{-1} apparently gains some intensity.

Figure 7c comes from the same film but after it has been transformed into a heavily reduced state and exposed to methanol at 390 K. The type I species are no longer present, and the peaks representing the type II and type III species in the ν(CO) region have shifted toward higher wavenumbers. Interestingly, the $\nu_a(CH_3)$ band at 2912 cm^{-1} is substantially

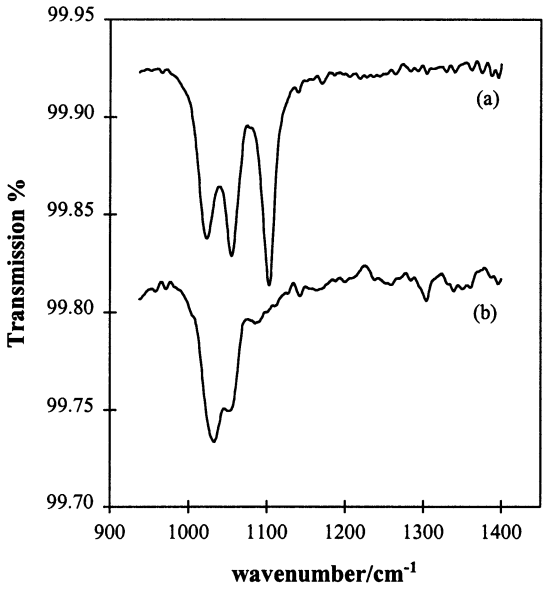

Figure 8. RAIRS spectra recorded at 300 K from a 10 ML annealed film dosed with CH_3OH to saturation coverage at (a) 300 K and at (b) 510 K.

reduced in intensity, indicating that it was principally the type I species that contributed to the band for this film. In the ν_s-(CH_3) region the peak maximum has also shifted, but in this case down in frequency from 2808 to 2790 cm^{-1}. These shifts may be compared with those reported in the literature,[18,19] which show that reduction of Ce^{4+} to Ce^{3+} led to a shift of 15 cm^{-1} of the ν(CO) bands toward higher wavenumbers and a downward shift of about 21 cm^{-1} for the $\nu_s(CH_3)$ band. As might be expected, the type I species can be regenerated, and the peaks of the type II and type III species shift back toward their original values if the same film is reoxidized; this is evident from Figure 7d, which was recorded after flashing the surface to 770 K and then exposing it to oxygen at 320 K (thereby generating a *preoxidized* surface) before again dosing methanol at the same temperature. Once the film has been reoxidized, additional postoxidation (Figure 7e) causes no further effects apart from the fact that a new small peak appears at 1080 cm^{-1}.

Figure 8b illustrates the effect of surface temperature on methanol adsorption. From spectrum b it is apparent that methoxy species are still the predominant surface species produced by methanol exposure even when this exposure is carried out at temperatures as high as 510 K. Furthermore, it appears that it is the type II and type III methoxy species that are the more thermally stable, since although the intensity of all the peaks is reduced compared to those from exposures at 320 or 390 K, peaks are still clearly discernible at 1058 and 1036 cm^{-1}, while the band at around 1100 cm^{-1} associated with type I species is virtually absent (once again the 2912 cm^{-1} band intensity is substantially reduced in the absence of type I species).

Additional peaks, not attributable to surface methoxy, were only observed on very rare occasions for thick oxide films; these were relatively weak peaks at 1373 and 2836 cm^{-1} in experiments that involved adsorption of methanol onto particularly highly oxidized films (as evidenced by the preponderance of the type I methoxy species).

2. The 3 ML Oxide. Figure 9 shows spectra recorded at 320 K from a 3 ML *annealed* film first exposed to a saturation dose of methanol and then subjected to increasing exposures of oxygen. In the initial spectrum, the ν(CO) region contains an intense peak at 1067 cm^{-1} and a much weaker peak at 1117

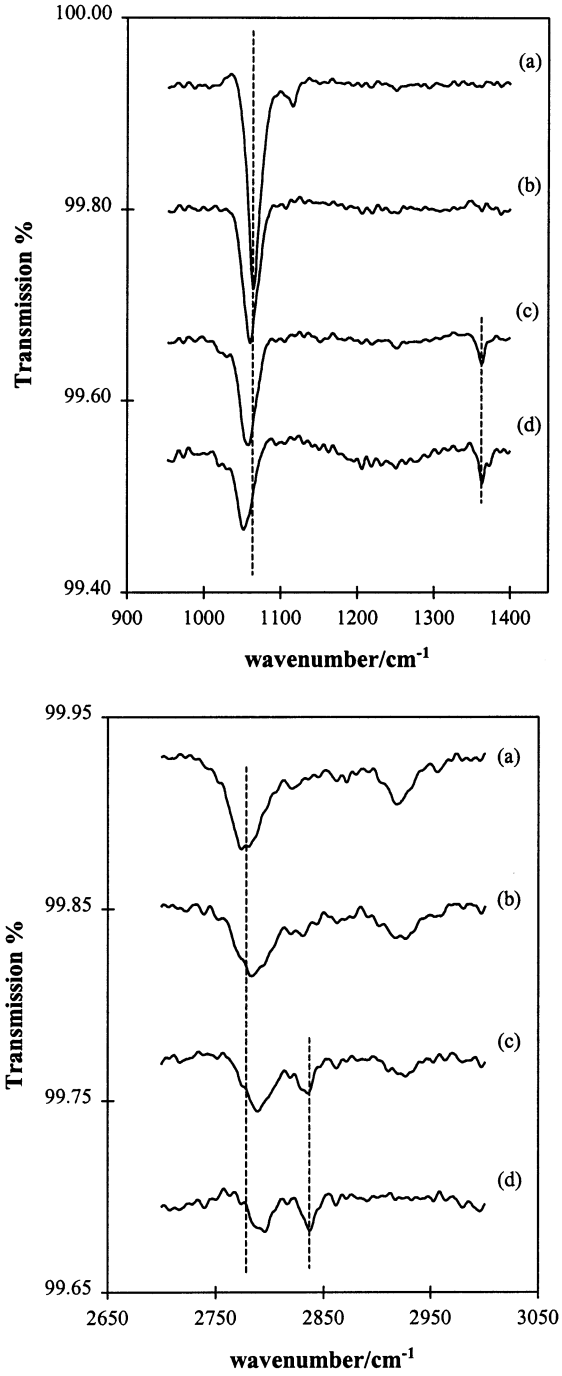

Figure 9. RAIRS spectra recorded at 300 K from a 3 ML annealed film: (a) dosed with CH_3OH to saturation coverage at 300 K and then exposed to (b) 1.8 L of O_2, (c) 3.4 L of O_2, and (d) 5.8 L of O_2.

cm^{-1}. This, in combination with the $\nu_s(CH_3)$ band observed at 2778 cm^{-1} and the $\nu_a(CH_3)$ peak at 2920 cm^{-1}, indicates that this surface is not well-oxidized and is almost exclusively covered with bridged type II methoxy species. In such circumstances the stepwise dosing of oxygen at 320 K has the following effects. The ν(CO) peak at 1067 cm^{-1} starts to shift toward lower wavenumbers and loses intensity such that after the highest oxygen exposure, the peak maximum has shifted to 1051 cm^{-1} and a substantial part of the intensity has been lost. The $\nu_s(CH_3)$ peak, originally at 2778 cm^{-1}, initially shifts to 2792 cm^{-1} and its intensity then drops away at higher oxygen doses. The $\nu_a(CH_3)$ peak, initially at 2920 cm^{-1}, apparently loses intensity more rapidly than the symmetric methyl stretch and becomes undetectably small at high oxygen doses. Simultaneous

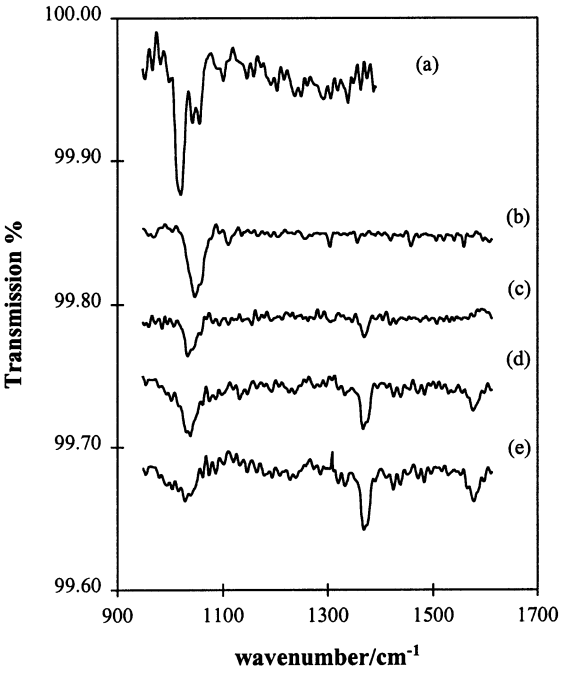

Figure 10. RAIRS spectra recorded at 300 K from a 0.70 ML: (a) fresh (unannealed) film dosed with CH_3OH to saturation coverage at 300 K; (b) annealed film dosed with CH_3OH to saturation coverage at 300 K and (c) subsequent exposure to 9 L of O_2; (d) preoxidized film dosed with CH_3OH to saturation coverage at 300 K and (e) subsequent exposure to 9 L of O_2.

with the decrease in intensity of these methoxy peaks, two new bands appear at 2834 and at 1363 cm^{-1}. The latter of these two new peaks also exhibits a shoulder at 1373 cm^{-1} at higher oxygen doses. These new bands may be assigned to the ν(CH) and the ν_s(OCO) vibration modes, respectively, of a formate species [see Discussion] as a result of the oxidation of methoxy species by surface oxygen. A small quantity of the same formate species may also be generated by adsorption of methanol at slightly elevated temperatures (e.g., at 420 K) onto a *preoxidized* surface.

3. The <1 ML Oxide. In this instance, the adsorption of methanol was also briefly studied on a fresh (never annealed) oxide film corresponding to a submonolayer coverage of ca. 0.7 ML. Spectrum a of Figure 10 shows that the main band is at ca. 1021 cm^{-1}, and it may therefore be attributed to triply bonded type III species on the oxide surface. There are also two smaller peaks at 1044 and 1057 cm^{-1}, of which the latter may be assigned to bridging type II methoxy species on the oxide on the basis of our results from the thicker oxide films, and $\nu(CH_3)$ bands at 2923 and 2785−2816 cm^{-1}.

Dosing methanol onto an *annealed* oxide of submonolayer coverage leads only to very weak absorption peaks (Figure 10b). The main ν(CO) peak has a maximum at 1048 cm^{-1} with a shoulder at 1059 cm^{-1}, the latter again clearly indicative of type II methoxy species on a partially reduced surface, and only the $\nu_s(CH_3)$ mode is evident with a peak maximum at ca. 2790 cm^{-1}. The 1048 cm^{-1} peak may be associated with type III species on the same reduced surface, although this is discussed further below. Postoxidation of this same surface (Figure 10c) causes the $\nu_s(CH_3)$ peak to disappear, and there is a clear reduction in the intensity of the peaks in the ν(CO) region accompanied by a shift in the peak maximum to ca. 1035 cm^{-1}, although there is still evidence for some absorption in the range 1045−1060 cm^{-1}. At the same time a new weak band appears at 1370 cm^{-1}, indicating that, as is the case with the 3 ML film, some of the methoxy species are transformed to formate species during the postoxidation procedure at 300 K.

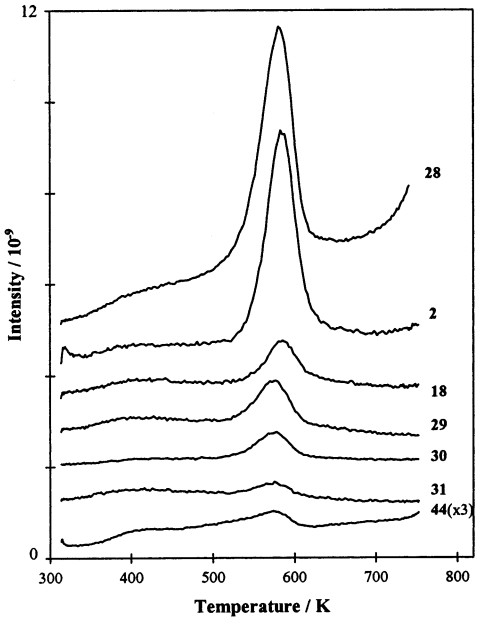

Figure 11. TPD multimass spectrum showing all the major desorption peaks from a well-oxidized annealed 10 ML ceria film after dosing of CH_3OH to saturation coverage.

After dosing methanol to saturation coverages on a *preoxidized* film of submonolayer coverage (Figure 10d), we only detect one broad peak originating from the vibrational modes of surface methoxy groups; this has a maximum at 1040 cm^{-1}. The other main band in this spectrum is at 1369 cm^{-1}, with a shoulder at 1376 cm^{-1}, and there are two weaker peaks at 1580 cm^{-1} and at ca. 2850 cm^{-1}; these peaks may be assigned to the ν_s(OCO) or δ(CH) mode, the ν_{as}(OCO) mode, and the ν(CH) mode, respectively, of a formate species. Postoxidation (Figure 10e) again causes a decrease in the intensity of the methoxy ν(CO) band, while the intensities of the remaining peaks increase, indicating that further oxidation of methoxy to formate species has occurred.

TPD Data. TPD spectra (Figure 11) recorded after dosing a saturation coverage of methanol onto thick *annealed* cerium oxide films are characterized by a series of peaks in the temperature range 550−600 K, most notably in the 2, 18, 28, 29, and 30 mass signals. These peaks are virtually coincident, indicative of the kinetics being controlled by the decomposition of a single surface intermediate, although small (<10 K) shifts between the peak maxima are consistently observed (the peak maxima in order of increasing temperature are 29, 30, 31, 32 < 28 ≈ 2 ≤ 18). The main carbon-containing product detected is carbon monoxide (CO) with a peak maximum at about 580−585 K. The ratio of the 29 and 30 amu signals shows that formaldehyde (HCHO) is also a significant product, while the relatively low intensity of the 31 and 32 amu signals indicates that methanol is only a minor product (since it is known from the RAIRS results that methanol dissociates completely on the oxide surface at room temperature, the traces of methanol detected during these TPD experiments must be a product of recombination). Surface hydrogen is a necessary byproduct of any dehydrogenation reaction leading to CO and HCHO, and this is evident from the simultaneous desorption of H_2 itself (2 amu) and H_2O (18 amu). Traces of CO_2 are also detected at around 425 and 575 K.

The TPD results from dosing of methanol onto an *oxygen-predosed* surface and from experiments in which the methanol-

saturated surface was then exposed to oxygen are very similar to those described above, with only very subtle differences in the peak profiles and relative peak intensities.

In every case, therefore, the TPD data are consistent with the following sequence of reactions taking place on the oxide surface:

adsorption, 300 K

$$CH_3OH_{(g)} + O_s \rightarrow CH_3O_{(ads)} + O_sH_{(ads)}$$

surface reactions/desorption processes, 575−590 K

$$CH_3O_{(ads)} \rightarrow CH_2O_{(g)} + O_sH_{(ads)} \quad \text{slow}$$

$$CH_3O_{(ads)} + O_sH \rightarrow CH_3OH_{(g)} + O_s \quad \text{fast}$$

$$CH_3O_{(ads)} \rightarrow CO_{(g)} + 3O_sH \quad \text{fast}$$

$$O_sH_{(ads)} + O_sH_{(ads)} \rightarrow H_{2(g)} + 2O_s \quad \text{fast}$$

$$O_sH_{(ads)} + O_sH_{(ads)} \rightarrow H_2O_{(g)} + O_s \quad \text{fast}$$

The traces of CO_2 that are observed could in principle arise from the decomposition of some surface carbonate species (perhaps formed by adventitious adsorption of CO_2 during methanol exposure) or from the decomposition of small amounts of formate species; however, the fact that the higher peak is coincident with those of the other desorption products suggests that this CO_2 may be reactively formed from the further oxidation of other surface species (e.g., formaldehyde) involved in the main series of reactions.

TPD spectra from thinner 3 ML oxide films show many of the same characteristics as reported above for the thicker oxide films. For example, Figure 12A shows desorption from a 3 ML *annealed* oxide film after dosing of methanol to saturation coverage at 350 K. Hydrogen is once again a major product, as is formaldehyde for which the desorption yield is now similar in magnitude to that of CO. Water and methanol, however, are now only seen in trace amounts. The main peaks are noticeably broader and more structured than for the thicker oxide films; the 2, 29, and 30 amu peaks have maxima at around 560 K with a high-temperature shoulder at ca. 580 K, whereas the CO peak maximizes at around 590 K but has a low-temperature shoulder at ca. 560 K. The data are therefore consistent with the occurrence of two similar reaction channels; the first leads to peak maxima at ca. 560 K and generates similar yields of formaldehyde and CO, and the second has characteristics virtually identical to that of the thicker oxide films (described above) with desorption peak maxima at ca. 585 K and CO as the predominant carbon-containing product.

The effects of preoxidation and postoxidation are much more marked for these thinner 3 ML films, as can be seen in parts B and C of Figure 12. In both cases the yield of *all* the major products in the range 500−600 K is lower than for the simple adsorption of methanol on the annealed oxide film. There is also a marked reduction in the intensity of the 2 amu peak relative to CO, but some water desorption is now evident at around 560 K. The main difference in the high-temperature chemistry, however, is the increase in the amount of CO_2 desorption with peaks evident in the 44 amu trace at 460 and 580 K. Comparison with the IR data indicates that at least one of these peaks is likely to be associated with the decomposition of surface formate species, with the hydrogen being removed either as molecular hydrogen (by recombination) or as water (following reaction with surface hydroxy species).

$$HCOO_{(ads)} \rightarrow H_{(ads)} + CO_{2(g)} \qquad (2)$$

Another feature that is particularly evident in Figure 12C is that small amounts of HCHO and hydrogen (2, 29, and 30 amu) desorb at about 370 K after dosing methanol to saturation coverage on a *preoxidized* 3 ML film at 300 K; the intensity of these low-temperature peaks is, however, very dependent on the exact temperature at which dosing is carried out (dosing at or below 300 K is required to really see these peaks) and on the history of the oxide film (the surface from which the data of Figure 12C were obtained had been repetitively heated to 773 K). This chemistry closely resembles that seen on partially oxidized copper surfaces,[20,21] and these observations are therefore taken to be indicative of the partial aggregation of the surface oxide after a large number of thermal cycles.

Oxide films of a submonolayer coverage exhibit very different behavior in TPD. The high-temperature coincident desorption peaks that are the main characteristic of the thicker oxide films are virtually absent. Weak coincident H_2 and CO peaks are just discernible at ca. 545 K for an annealed film, but only the CO peak (and no H_2 or H_2O) is evident when the surface is subject to either pre- or postoxidation, and once again, the amount of CO desorbing at this temperature is very small. With the exception of the weak H_2 and CO peaks, the desorption traces from an annealed submonolayer oxide surface are virtually featureless. By contrast, dosing of methanol onto a preoxidized surface or postoxidation also gives rise to a CO_2 desorption peak maximizing at 490−510 K, small amounts of H_2 desorption at 340−370 K, and formaldehyde desorption (and trace levels of methanol) at ca. 390 K (Figure 13). The CO_2 desorption may again be attributed to decomposition of a surface formate (in accord with the IR data but see below for more discussion on the nature of this species), and as noted above for the 3 ML data, the low-temperature hydrogen and formaldehyde peaks are consistent with the known reactions of methanol on oxidized copper surfaces.

Discussion

Atomistic computer simulation techniques have been used by other workers to model various single-crystal surfaces of ceria, with attention given to their structures and relative stability as well as to the energetics of creation of anion vacancies on the surfaces.[22,23] These calculations predict the close-packed (111) surface to be the most stable at 273 K and less prone to accommodate a vacancy defect than other surfaces, although pairing of vacancies does seem to be favored. The last point implies that even if surface anion vacancies are only generated at low concentration by reduction, they will tend to readily form pairs. In fact, scanning tunneling microscopy (STM) studies appear to indicate that the formation of a vacancy trimer is still more favored.[24] In the absence of any reconstruction, the (111) surface of the oxide should have a hexagonal unit cell with a size of 3.825 Å (based on the cubic unit cell constant of the bulk oxide of $a_o = 5.411$ Å[25]). This is in excellent agreement with the observed hexagonal (1.5×1.5) overlayer structure, which has a lattice parameter $a = 3.84 \pm 0.11$ Å, and on this basis, the oxide films grown in this study are taken to have a CeO_2(111)-like structure.

The (111) surface can be considered as being formed by a stacking of O−Ce−O sandwiches,[26] terminating in a layer of oxygen anions. In the absence of surface vacancies all the oxygen anions exposed at the surface are bonded to three of the underlying Ce^{4+} cations, which are in turn seven-coordinated. In the bulk of the oxide the Ce^{4+} cations are symmetrically surrounded by eight oxygen anions; the cations adjacent to the surface are thus deficient of one anion from their

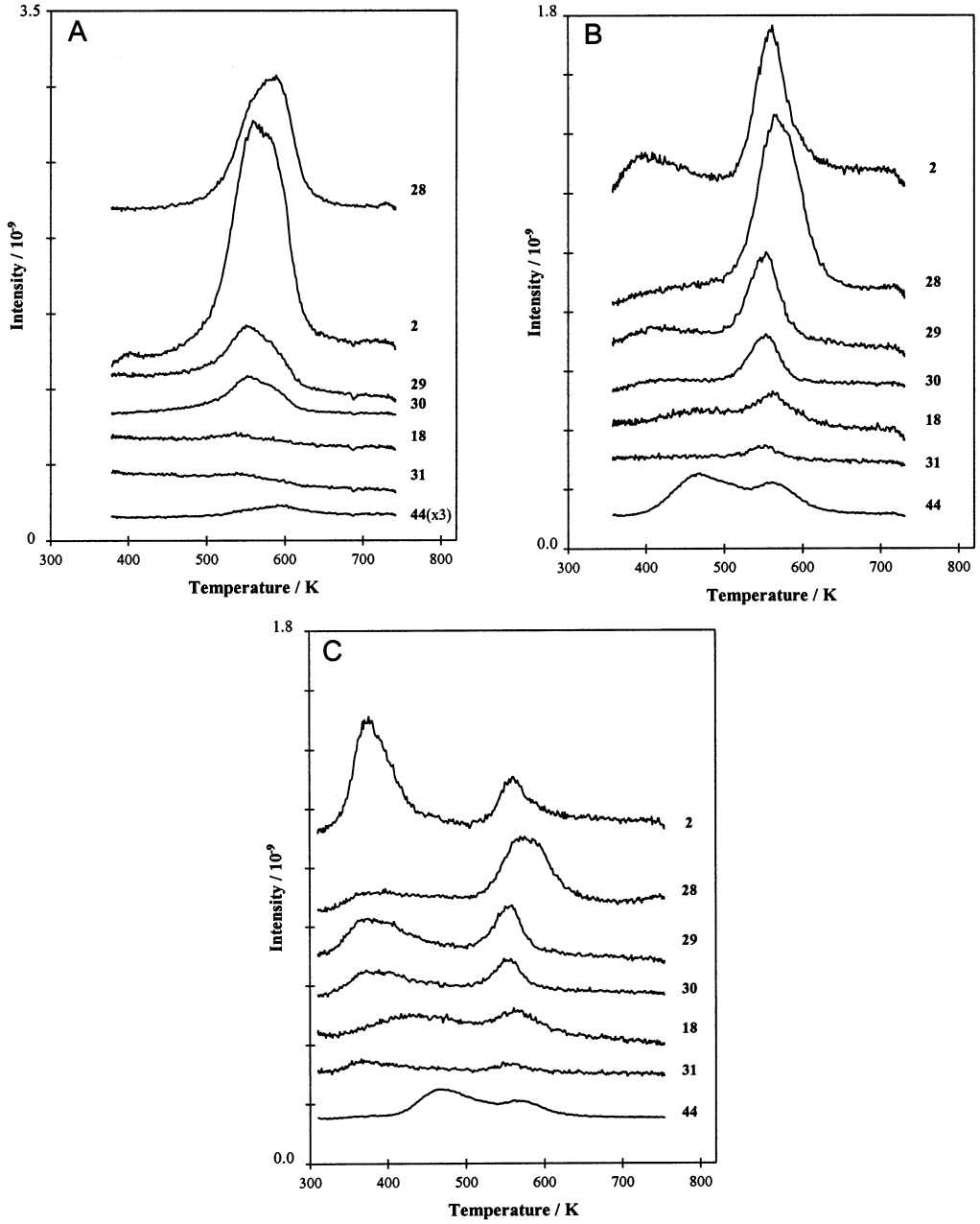

Figure 12. TPD multimass spectra showing desorption from a 3 ML oxide film after the following treatments: (A) annealed film dosed with CH_3OH to saturation coverage; (B) annealed film dosed with CH_3OH to saturation coverage and with subsequent oxidation; (C) preoxidized film dosed with CH_3OH to saturation coverage and with subsequent oxidation.

first coordination sphere, and it is to be expected that a methoxy species can fill this vacant site (Figures 14 and Figure 15A). In so doing they are binding to a single Ce^{4+} cation and are therefore the type I species to which we have previously referred.

The hydrogen liberated during the dissociative adsorption of the methanol molecule may bond to a surface oxide ion, thereby forming a hydroxy species as indicated in reaction 1. The only evidence that this hydrogen does indeed remain on the surface is from other closely related studies, specifically, that (i) hydrogen is not observed as a gas-phase product when methanol is beamed onto a $La_2O_3(001)$ surface at 300 K [27] and (ii) TPD studies of CD_3OH adsorption on ceria films on Pd(111) reveal H atom incorporation into the coincident desorption products at high temperatures.[28] Since all oxide ions on the (111) surface are initially bonded to three underlying Ce^{4+} cations, any hydroxy species formed by methanol adsorption are presumed to be coordinated in a similar fashion. This does present the possibility that site exchange between hydroxy and methoxy groups (alternatively viewed as an exchange of H and methyl groups) might lead to the formation of type III methoxy groups in which the methoxy is now bound to three Ce^{4+} cations, even on well-oxidized surfaces where such species might not otherwise be expected. We have no definitive evidence for this process, although we do have a number of spectra from well-oxidized thick films in which the absorption band associated with type III species is markedly more intense than the type II band (Binet et al.[29] also report observing a triply bonded species on very well-oxidized ceria with a characteristic IR band at 1016 cm^{-1}).

When oxygen vacancies are present on the surface, as they must be to some extent at any temperature above absolute zero, then additional binding geometries for the surface methoxy species are possible in which the methoxy group is bonded in a bridging fashion to either two or three cations (type II or type

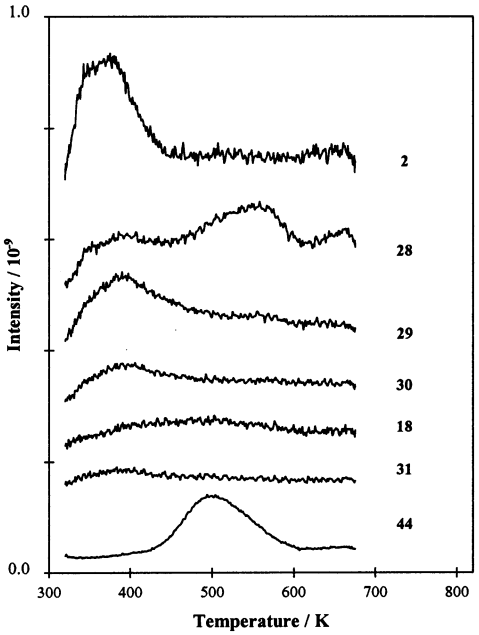

Figure 13. TPD data showing desorption from a preoxidized surface of submonolayer oxide thickness after dosing CH_3OH to saturation coverage.

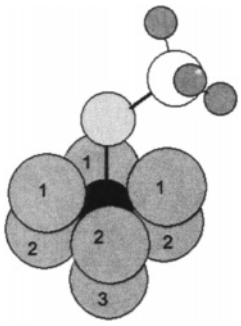

Figure 14. Schematic representation of an on-top (type I) methoxy species bonded to a Ce^{4+} cation (black sphere). The oxygen ions (grey spheres) of the first coordination shell of this cerium ion are also shown with numbers to indicate the $O^{2-}(111)$ lattice plane in which they are located.

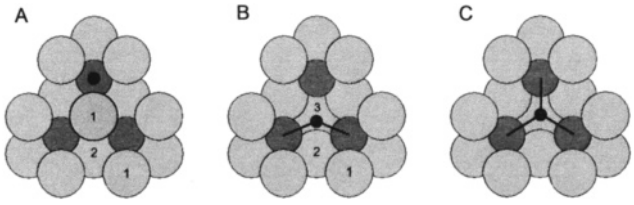

Figure 15. Plain view of the $CeO_2(111)$ surface. The light and dark-gray circles represent oxygen and cerium ions, respectively, while the black spot and associated rods are used to illustrate the position and local coordination geometry of the O atom of a methoxy group: (A) on-top (type I) species in the absence of oxygen vacancies; (B) bridging (type II) and (C) triply bridging (type III) species, respectively, in association with an oxygen ion vacancy.

III species, respectively) as illustrated in Figure 15. The XPS data clearly confirm that the creation of oxygen vacancies must involve a reduction of some Ce^{4+} ions to Ce^{3+} ions. Furthermore, calculations indicate that the Ce^{3+} ions are always in direct contact with the vacancies and preferentially occupy the lower coordination sites when the vacancies are clustered.[23] The type II and type III methoxy species generated at oxygen vacancies may therefore be coordinated either to solely Ce^{3+} ions or to a mixture of Ce^{3+} and Ce^{4+} ions.

Certain characteristics of the surface methoxy groups generated by methanol dissociation are sensitive to the exact nature of the surface coordination site; of most relevance to this work, this sensitivity clearly extends to the vibrational mode frequencies of the adsorbed species. Of the various vibrational modes, the ν(CO) mode is particularly sensitive to the surface coordination, which is to be expected, since it is the oxygen atom that is directly bound to the surface. More specifically, the frequency of the ν(CO) mode can reveal the bonding geometry to the cationic sites and, furthermore, permits one to qualitatively follow the reduction state of the ceria surface. The $\nu(CH_3)$ mode frequencies are influenced to a much lesser extent by the adsorption site; nevertheless, the shift of the $\nu_s(CH_3)$ band to lower wavenumbers can again be used as a qualitative index for the reduction state of the ceria surface. Using this approach, Bardi et al.[18] have identified on-top and doubly and triply coordinated methoxy species after methanol adsorption at room temperature on microporous and nonmicroporous ceria samples. Furthermore, upon reduction they observed that the on-top methoxy species were entirely transformed to doubly bridged ones, indicative of complete surface reduction.

In Table 1 we summarize the vibrations of methoxy species detected during our RAIRS measurements on both well-oxidized ceria films and on films containing a large number of surface vacancies (data for methanol on the oxidized Cu(111) surface is also included for comparison). The assignments are in the main based on the aforementioned work of Bardi et al.,[18] but we make the following additional points of justification.

(i) The effect of surface coordination number is most evident on the ν(CO) frequency. This indicates that the shifts seen in this mode are primarily related to changes in the effective mass of the metal−oxygen complex; as the coordination of the oxygen is increased, the effective mass increases and the frequency of the ν(CO) stretch is correspondingly reduced. The frequencies of modes centered on the methyl groups, which involve only minor displacements of the other atoms of the adsorption complex, are much less sensitive to the coordination of the oxygen.

(ii) Frequency shifts induced by the extent of surface oxidation/reduction may be modeled by considering the effect of varying the amount of negative charge localized on the oxygen of the methoxy group. Simple valence bond representations indicate that as the negative charge on the oxygen increases (corresponding to a change in the oxidation state of the metal atom(s) from Ce^{4+} to Ce^{3+}, on the basis that Ce^{4+} will tend to polarize and delocalize this charge more effectively than Ce^{3+}), then the C−O bond order and ν(CO) stretch frequency will increase while the methyl group frequencies will decrease. These conclusions are supported by accurate theoretical calculation. A comparison of the vibrational frequencies of the methoxy radical ($CH_3O^{\bullet}$) and the methoxide anion (CH_3O^-), both calculated at the DFT-B3YLP/6-311+G(2d,p) level, shows that as the negative charge of the molecular entity is increased from 0 to 1, then there is a shift in the ν(CO) stretching mode to higher frequency (by ca. 35−40 cm^{-1}) and a very substantial decrease in the $\nu(CH_3)$ stretch mode frequencies (by several hundred cm^{-1}).

For the oxide films employed in these studies (which are at maximum 20 ML thick), we would still expect the surface dipole selection rule to be in effect;[30] if so, then the observation of the antisymmetric methyl stretch vibration indicates that the O−C axis of the methoxy group concerned is not perpendicular to the underlying metallic surface. Considering our data as a whole, it is clear that intensity in the asymmetric stretch arises as a

TABLE 1: Summary of Observed Vibrational Frequencies for Methoxy Species on Cerium Oxide and Cu(111) Surfaces

vibrational mode	O−CH_3 (I) well-oxidized (cm^{-1})	O−CH_3 (II) well-oxidized (cm^{-1})	O−CH_3 (III) well-oxidized (cm^{-1})	O−CH_3 (I) reduced (cm^{-1})	O−CH_3 (II) reduced (cm^{-1})	O−CH_3 (III) reduced (cm^{-1})	O−CH_3 O/Cu(111)[c] (cm^{-1})
$\nu_a(CH_3)$	2912	2925	(2925)[a]		2916		2911
$2\delta(CH_3)$							2881
$\nu_s(CH_3)$	2808	2793	2793		2780	2780	2808
$\rho(CH_3)$							1134
ν(CO)	1105	1054	1025 (1015[b])	1117	1067	1045	1046

[a] This peak could be masked by that due to type II species (or may be surface dipole forbidden). [b] A small amount of triply bonded species may be generated on well-oxidized surfaces by H/CH_3 exchange. [c] In this case methanol was dosed onto a Cu(111) surface that had first been treated by exposure to 270 L of O_2 at 573 K.

result of both type I and type II methoxy groups, although on the thicker (>5 ML) oxide films the main contribution is clearly from the type I species (consistent with our expectation that this species will be tilted with respect to the surface normal; see Figure 14). Type II species adsorbed at a single oxygen vacancy site on the (111) surface (Figure 15B) are also expected to have the molecular plane (defined by the C, O, and two Ce atoms) tilted with respect to the surface normal, but this requirement is relaxed if the oxygen vacancies are clustered, which might explain why their contribution to the asymmetric band is relatively weak. We are not able to say from the experimental data whether the type III species contribute in any way to this antisymmetric band, but a simple geometrical model of the type III adsorption complex would lead to a prediction of C_{3v} symmetry, with the C−O bond perpendicular to the oxide (111) surface and hence also to the metal surface, in which case the asymmetric stretch would be symmetry-forbidden.

As noted earlier, even when the adsorption of methanol was carried out on well-oxidized, thick CeO_x films, the IR spectra generally reveal all three types of methoxy species (see, for example, Figure 7a). If no oxygen vacancies were present, then one would expect to see only the band at ca. 1108 cm^{-1} corresponding to on-top methoxy groups; instead the presence of peaks at 1058 and 1027 cm^{-1} in the ν(CO) region is a clear indication that some oxygen ion vacancies are still present on such a surface. This is confirmed by the Ce 3d XP spectra where at grazing emission angles we can detect Ce^{3+} characteristics (Figure 3). Postoxidation will result in a filling of some of these oxygen vacancies and a consequent displacement of some of the bridged type II species to the on-top position. This is clearly evident in a direct comparison of spectra a and b of Figure 7, but the fact that we detect only small shifts in peak positions and relative intensities from the previous state indicates that the change in the surface oxidation state induced by the postoxidation is small. Furthermore, the surface chemistry is not strongly influenced by the exact concentration of surface vacancies, since the TPD results obtained after methanol adsorption on annealed, preoxidized and postoxidized thick oxide films do not exhibit major differences. To summarize, since not all the type II and type III bridged species are converted into on-top type I species, it appears that postoxidation does not create a surface completely free from vacancies. However, it should be noted that the above observations do not exclude the possibility that some of the bridged species could be present at step sites of the oxide surface and that these step sites are not "deactivated" to bridging coordination of methoxy groups by the oxidation procedures. In rare cases on a well-oxidized thick film we did detect IR absorption bands originating from formate species formed from methoxy groups at room temperature on the oxide surface, and this may be indicative of the presence of such step sites (see below).

On a heavily reduced surface (such as that pertaining to Figure 7c), the concentration of oxygen vacancies in the surface layer will be much higher and almost all of the first layer of cerium ions are expected to be reduced to Ce^{3+}. This is supported by our observations that the peak originating from type I on-top methoxy species is absent, the ν(CO) peak positions for the bridging methoxy groups are shifted toward higher wavenumbers, and the $\nu(CH_3)$ peaks are shifted to lower wavenumbers. Postoxidation (not shown) causes the ν(CO) bands to shift back slightly to lower wavenumber, indicating a partial oxidation of the surface, and there is also some transformation from bridged to on-top species. However, the oxidation of the surface is much more effective if the methanol is first flashed away prior to the exposure to oxygen; when methanol adsorption is subsequently carried out, the band representing the on-top methoxy species is then once again the most intense, as shown in Figure 7d.

Li et al.[31] studied the surface species formed from the adsorption and decomposition of methanol on dehydroxylated polycrystalline ceria, from 300 to 673 K, using FTIR. They found that some methoxy species were oxidized to give formate species, after heating of the cerium oxide to 473 K. These formate species were found to gradually decompose at 573 K. This conversion of methoxy to formate was not readily observed in our own work on the CeO_2(111)-type surface exhibited by the *thick* oxide films. By contrast, in our experiments on the 3 ML oxide films, postoxidation at 300 K of an annealed surface covered with methoxy species is seen to cause oxidation of some of the methoxy groups to formate species and dosing of methanol onto a preoxidized surface at slightly elevated temperatures also generates the same formate species. Although it has been noted that there may be some underlying copper surface exposed with such 3 ML films, we attribute the new IR bands to a bidentate formate species associated with the surface of the oxide and not to formate species on copper. The main evidence for this is as follows: (1) the formation of the formate is clearly associated with the consumption of methoxy species, which are unambiguously identified as being located on the oxide; (2) the observed vibrational mode frequencies are in excellent agreement with those reported by Li et al.[31] for a bidentate formate on pure ceria and for one of the two formate species observed by ourselves after dosing formic acid onto very thick oxide films (see Table 2); (3) the same formate may be formed from methanol on much thicker oxide films provided the oxidation state of such films is very high.

If the oxide film is an annealed one (as in the case of Figure 9 and Figure 10c), the reaction to form formate takes place during the postoxidation procedure. If the film is preoxidized as in Figure 10d, then the reaction may take place directly when dosing methanol. The reaction can take place at 300 K but may be enhanced by raising the substrate temperature slightly.

The fact that the $\nu_a(CH_3)$ band of methoxy disappears almost completely as soon as the bands due to the formate species

TABLE 2: Summary of Observed Vibrational Frequencies for Formate Species on Cerium Oxide and Cu(111) Surfaces

vibrational mode	CH_3OH 3 ML of CeO_x (cm^{-1}) this work	CH_3OH <1 ML of CeO_x (cm^{-1}) this work	CH_3OH poly-CeO_x (cm^{-1}) ref 31	HCOOH poly-CeO_x (cm^{-1}) ref 31	HCOOH multi-CeO_x (cm^{-1}) this work	HCOOH O/Cu(111) (cm^{-1}) this work[c]	Na^+HCOO^- (cm^{-1}) ref 33
ν(CH)	2838	2850	2846	2845	2890 2845	2931 2848	2841
					2178[b]	2181[b]	
ν_a(OCO)		1580	1547	1599 1553 1542	1616[a] (tailing to low cm^{-1})		1567 1542
ν_s(OCO), δ(CH)	1374 (sh) 1364	1376 (sh) 1369	1376	1371 1362 1248	1300[a] 1378[a]	1352 1334 (sh)	1377 1366
δ(OCO)				777	768		772

[a] These bands are believed to correspond to at least two species: a monodentate formate giving rise to strong bands at 1300 and 1616 cm^{-1} and a bidentate formate with a strong band at 1378 cm^{-1} and a much weaker band just below 1600 cm^{-1}. [b] The band at 2178−2181 cm^{-1} cannot be assigned to a fundamental vibration of adsorbed formate; it is a good match to the CO stretch mode of the formyl cation (HCO^+), which is seen at 2184 cm^{-1} in the gas phase.[32] [c] In this case formic acid was dosed onto a Cu(111) surface that had first been treated by exposure to 270 L of O_2 at 573 K. sh = shoulder.

appear indicates that the methoxy groups that are oxidized to formate are principally those that have the C−O axes inclined to the underlying metal surface. We also need to address why these formate species appear to be much more readily formed on the 3 ML oxide films than on thicker oxide films. We propose that this is principally related to the morphology of the oxide films. The thick oxide films are coherent (in the sense that no copper surface is exposed) and expose predominantly the (111) oxide surface, which is coplanar with the underlying Cu(111) surface. By contrast we know from the XPS results (Figure 4) that oxide films with thickness less than 5 ML start to aggregate above 600 K; after several annealing cycles such films (and especially the film of Figure 9, which has been annealed at 673 K) will exhibit more of an island morphology with large well-ordered oxide patches of several monolayers thickness but also with some bare copper exposed from the substrate. The peripheral regions of these islands must differ in orientation from the (111) surface of the "top" of these islands; the island edges may therefore either expose microfacets of a different crystallographic orientation and structure or be regions of a much higher step density. Furthermore, the oxygen ions present in this region are likely to be somewhat more labile and reactive than those on the close-packed (111) terrace. Any methanol adsorbing in this region will tend to generate methoxy groups that by necessity are more inclined to the underlying metal surface; in particular, it appears from our results that the type II bridging methoxy groups adsorbed at such sites contribute more to the $\nu_a(CH_3)$ band intensity, and on a well-oxygenated surface a small part of these methoxy species may be oxidized to formate. The extent of oxidation (i.e., the proportion of methoxy groups converted to formate) will be determined by the exact surface oxygen activity, which is in turn related to pre- and postoxidation treatments.

The formation of these formate species is apparent in TPD from the desorption of CO_2, although it is not immediately clear whether just one or both of the two peaks (at ca. 460 and 580 K) arise from formate decomposition. Our only other evidence comes from previous studies of dosing of HCOOH onto ceria films grown on Pd(111) in which it was observed that surface formate decomposed to yield a mixture of CO, CO_2, H_2, H_2O, and HCHO, all simultaneously desorbing with a peak temperature of 540−600 K, depending on the exposure and oxide film thickness.[28] This would suggest that the higher temperature CO_2 peak seen on the 3 ML oxide films is associated with formate decomposition and furthermore that methoxy and formate decompose in the same temperature range and yield a fairly similar range of products, i.e., that some of the other desorbing species in this temperature range may also be associated with formate decomposition. We would stress, however, that both the high-temperature decomposition channels previously referred to are still evident on annealed surfaces under conditions where only surface methoxy is observed, so it would be too simplistic to associate one channel with formate decomposition and one with methoxy decomposition. Instead we propose that it is the remaining un-oxidized methoxy species adsorbed in this perimeter region that decompose at a slightly lower temperature than those on the flat (111) surface; that is, that these are the species that follow the low-temperature reaction channel, described in the results section, which leads to similar yields of formaldehyde and CO at about 560 K. The other methoxy species that are adsorbed on the flat (111) surfaces of the oxide islands follow the same higher temperature reaction channel as seen on the thick oxide films (yielding peak maxima at ca. 590 K) with CO as the main product. The lower temperature reaction channel is not obvious on the thicker oxide surfaces, since the change in the morphology of the films means that such sites are eliminated.

For all the multilayer oxide films (i.e., >10 and 3 ML) it should be noted that the methanol adsorption capacity is higher on the annealed surface than on the corresponding preoxidized surfaces; this is evident from the high-temperature CO peak intensity in TPD, which, for example, is much larger in parts A and B of Figure 12 (which involve adsorption on annealed films) than in Figure 12C (a preoxidized film). The presence of surface oxygen vacancies therefore enhances the amount of methanol that can be accommodated on the surface. As might be expected, the oxygen availability also influences the relative desorption yields of water and hydrogen.

Another feature worthy of comment relates to the apparent conversion of some Ce^{4+} to Ce^{3+} upon exposure of the surface to methanol, as witnessed in XPS (Figure 6B). If this phenomenon were solely associated with the oxidation of some methanol to formate, then we would not expect to see such changes on annealed oxide surfaces, indicating instead that it may arise directly from the adsorption of methanol. This is understandable if the nature of the species arising from the dissociative adsorption of methanol is examined more carefully. If the fission of the C−O bond is considered heterolytic to generate a proton (which can then combine with a surface oxide ion) and the methoxide ion and if there is no further electron transfer, then

the oxidation state of cerium is retained:

$$Ce^{4+} + O^{2-} + CH_3OH \rightarrow Ce^{4+} + HO^- + CH_3O^- \quad (3)$$

Alternatively, if there is additional electron transfer from the methoxide ion to the cerium or if the whole adsorption process is considered from the point of view of a concerted radical-type mechanism involving homolytic fission of the C−O bond, then the cerium may be reduced to the Ce^{3+} state:

$$Ce^{4+} + O^{2-} + CH_3OH \rightarrow Ce^{3+} + HO^- + CH_3O^{\bullet} \quad (4)$$

To the extent that the IR spectra of adsorbed methoxy are much more closely related to those of the methoxy radical than the anion, then the experimental data support this latter interpretation.

The adsorption of methanol on oxide films of a submonolayer coverage requires special attention, since in this case there is a clear possibility of adsorption and surface reaction occurring on both the oxide surface and the exposed Cu(111) surface. The IR data do not provide good discrimination between methoxy groups on an oxidized copper surface and the various species observed on the cerium oxide; in particular, the most intense and easily observed ν(CO) band, which is expected at ca. 1045 cm^{-1} for methoxy on copper, overlaps the same band for some of the methoxy species expected on the oxide (see Table 1). It is likely, therefore, that some of the methoxy groups evident in Figure 10 are actually present on the copper surface, which would be consistent with the observation of formaldehyde desorption at ca. 370 K in TPD experiments from these surfaces. It is equally clear that most of the IR absorption intensity (in particular, the 1021 cm^{-1} band in Figure 10a, the shoulder at 1059 cm^{-1} and at least part of the 1048 cm^{-1} band in Figure 10b) is still associated with methoxy groups on the oxide. Once again, this is confirmed by the observation of some coincident H_2 and CO desorption in TPD data.

The nature of the formate species produced on these submonolayer oxide films by oxidation again requires close investigation. There are some differences between the peaks observed on this surface and those observed for the 3 ML oxide surface; the ν(CH) and ν_s(OCO) bands are slightly higher in frequency, and the ν_a(OCO) mode is now clearly apparent, but the spectrum is nevertheless still much more closely related to that for a bidentate formate on the oxide than to formate on copper. The spectrum is, however, also very similar to that reported for the formate ion in ionic salts, and given the very low nominal surface coverage of the oxide, this formate species is therefore probably better regarded as being associated with an ionic $Ce^{3+}/O^{2-}/HCOO^-$ surface complex supported on the copper surface rather than associated with formate adsorbed on an oxide surface. This subtle change in the nature of the formate as the oxide coverage is reduced is also reflected in the TPD data, where the peak temperature for CO_2 evolution is seen to shift to ~490 K, which is more akin to values previously reported for formate decomposition on an oxidized Cu(111) surface[21] and suggests that the copper surface now has a direct role in mediating the decomposition of the complex.

Conclusions

Well-ordered cerium oxide layers, exhibiting a CeO_2(111)-like epitaxial structure, may be prepared on a Cu(111) substrate and the Ce/O stoichiometry of the oxide controlled by careful selection of the growth mode, annealing, and oxidation conditions. Grazing emission XPS indicates that some Ce^{3+} ions are still present in the surface layers at 300 K after oxidation treatments and the presence of oxygen vacancies in the surface layer is confirmed by IR measurements after exposure to methanol vapor. Methanol is adsorbed dissociatively onto the ceria surface at 300 K to give predominantly surface methoxy species, and the IR spectra of these methoxy groups are a very useful tool for probing the structural and chemical nature of the oxide surface. Some surface methoxy groups may be oxidized to surface formate by a reaction that proceeds most readily at lower coordination sites near the perimeter of oxide islands rather than on the (111) surface itself. Both the methoxy groups and formate species are thermally decomposed below 600 K, with the former yielding a mixture predominantly of CO, H_2, and HCHO, while the latter process is also characterized by some CO_2 desorption. The decomposition temperature of the methoxy groups is slightly lower at sites near the edges of the oxide islands than on the (111) surface of thicker oxide films, and the copper surface itself can mediate the decomposition processes at very low oxide coverages.

Acknowledgment. Financial support in the form of an EC-TMR grant (ERBFMBICT 961039) for A.S. is gratefully acknowledged. Our thanks are also to Dr. P. A. Hamilton for carrying out DFT calculations on various adsorbed species to support the vibrational assignments.

References and Notes

(1) Yao, H.; Yao, Y. *J. Catal*. **1984**, *86*, 254.
(2) Morterra, C.; Balis, V.; Magnacca, G. *J. Chem. Soc., Faraday Trans*. **1996**, *92*, 1991.
(3) Kraus, K.; Schmidt, L. *J. Catal.* **1993**, *140*, 424.
(4) Kim, G. *Ind. Eng. Chem. Prod. Res. Dev.* **1982**, *21*, 267.
(5) Maruya, K.; Takasawa, A.; Aikawa, M.; Haraoka, T.; Domen, K.; Onishi, T. *J. Chem. Soc., Faraday Trans.* **1994**, *90*, 911.
(6) Lee, G. u.d.; Ponec, V. *Catal. Rev. Sci. Eng.* **1987**, *29*, 183.
(7) Nix, R. M.; Rayment, T.; Lambert, R. M.; Jennings, J. R.; Owen, G. *J. Catal*. **1987**, *106*, 216.
(8) Lamonier, C.; Bennani, A.; D'Huysser, A.; Aboukais, A.; Wrobel, G. *J. Chem. Soc., Faraday Trans.* **1996**, *92*, 131.
(9) Levoguer, C. L.; Nix, R. M. *Surf. Sci.* **1996**, *365*, 672.
(10) Alexandrou, M.; Nix, R. M. *Surf. Sci.* **1994**, *321*, 47.
(11) Hardacre, C.; Roe, G. M.; Lambert, R. M. *Surf. Sci.* **1995**, *326*, 1.
(12) Creaser, D. A.; Harrison, P. G.; Morris, M. A.; Wolfindolle, B. A. *Catal. Lett.* **1994**, *23*, 13.
(13) Braaten, N. A.; Grepstad, K. J.; Raaen, S. *Phys. Rev. B* **1989**, *40*, 7969.
(14) Romeo, M.; Bak, K.; El Fallah, J.; Le Normand, F.; Hilaire, L. *Surf. Interface Anal.* **1993**, *20*, 508.
(15) Belton, D. N.; Schmieg, S. J. *J. Vac. Sci. Technol. A* **1993**, *11*, 2330.
(16) Barteau, M. *J. Vac. Sci. Technol. A* **1993**, *11*, 216.
(17) Lamotte, J.; Moravek, V.; Bensitel, M.; Lavalley, J. C. *React. Kinet. Catal. Lett.* **1988**, *36*, 113.
(18) Bardi, A.; Binet, C.; Lavalley, J. C. *J. Chem. Soc., Faraday Trans*. **1997**, *93*, 1159.
(19) Binet, C.; Bardi, A.; Lavalley, J. C. *J. Phys. Chem*. **1994**, *98*, 6392.
(20) Fu, S. S.; Somorjai, G. A. *J. Phys. Chem.* **1992**, *96*, 4542.
(21) Russell, J. N., Jr.; Gates, S. M.; Yates, J. T., Jr. *Surf. Sci.* **1985**, *163*, 516.
(22) Sayle, T.; Parker, S.; Catlow, C. R. A. *Surf. Sci*. **1994**, *316*, 329.
(23) Conesa, J. C. *Surf. Sci.* **1995**, *339*, 337.
(24) Noremberg, H.; Briggs, G. A. D. *Surf. Sci.* **1998**, *404*, 734.
(25) Eyring, L. In *Handbook of Physics and Chemistry of Rare Earths*; Gschneider, K. A., Eyring, L., Eds.; North-Holland: Amsterdam, 1979.
(26) Bertaut, F. *Compt. Rend*. **1958**, *246*, 3447.
(27) De Asha, A. M.; Critchley, J. T. S.; Siokou, A.; Nix, R. M. Manuscript in preparation.
(28) Alexandrou, M. Ph.D. Thesis, University of London, 1993.
(29) Binet, C.; Jadi, A.; Lavalley, J. C. *J. Chim. Phys.* **1992**, *89*, 1441.
(30) Bradshaw, A. M.; Richardson, N. V. *Pure Appl. Chem*. **1996**, *68*, 457.
(31) Li, C.; Domen, K.; Marua, K.-I.; Onishi, T. *J. Catal.* **1990**, *125*, 445.
(32) Liu, D. J.; Lee, S. T.; Oka, T. *J. Mol. Spectrosc.* **1988**, *128*, 236.
(33) Ito, K.; Bernstein, H. J. *Can. J. Chem.* **1956**, *34*, 170.